City Research Online

City, University of London Institutional Repository

**Citation:** Kumar, N., Khader, S. M. Abdul, Pai, R., Khan, S. H. & Kyriacou, P. A. (2020). Fluid structure interaction study of stenosed carotid artery considering the effects of blood pressure. International Journal of Engineering Science, 154, 103341. doi: 10.1016/j.ijengsci.2020.103341

This is the accepted version of the paper.

This version of the publication may differ from the final published version.

**Permanent repository link:** https://openaccess.city.ac.uk/id/eprint/24465/

**Link to published version:** https://doi.org/10.1016/j.ijengsci.2020.103341

**Copyright:** City Research Online aims to make research outputs of City, University of London available to a wider audience. Copyright and Moral Rights remain with the author(s) and/or copyright holders. URLs from City Research Online may be freely distributed and linked to.

**Reuse:** Copies of full items can be used for personal research or study, educational, or not-for-profit purposes without prior permission or charge. Provided that the authors, title and full bibliographic details are credited, a hyperlink and/or URL is given for the original metadata page and the content is not changed in any way.

City Research Online: http://openaccess.city.ac.uk/ publications@city.ac.uk

# Fluid Structure Interaction Study of Stenosed Carotid Artery Considering Effect of Blood Pressure

Nitesh Kumar[1, 2], R Pai[1], S M Abdul Khader[1], S H Khan[2], P A Kyriacou[2]

[1]Department of Mechanical and Manufacturing Engineering, Manipal Institute of Technology, Manipal Academy of Higher Education

[2]School of Mathematics and Computer Science Engineering, City, University of London, London, UK.

Corresponding Author: R Pai

**Abstract**: Atherosclerosis is the most common Cardiovascular Disease (CVD) causing increased morbidity. Although atherosclerosis is a general disease involving several factors, it preferentially affects the wall of the vessel bifurcations. The employment of advanced Computational Fluid Dynamics (CFD) has the potential in shedding more light in the further understanding of the causes of the diseases and perhaps aid in the early diagnosis. In this study, a three-dimensional Fluid Structure Interaction (FSI) study was carried out for a patient specific carotid. By considering physiological conditions, first normal and then with hypertension disease, hemodynamic parameters are evaluated to better understand the genesis and progress of atherosclerotic plaques in the carotid artery bifurcation. Two-way FSI was performed by applying a fully implicit second-order backward Euler differencing scheme using commercial code ANSYS and ANSYS CFX (version 19.0). Arbitrary Lagrangian–Eulerian (ALE) formulation is employed to calculate the arterial response by using the temporal blood response. Due to arterial bifurcation, obvious velocity reduction and backflow formation is observed which decrease shear stress and made it oscillatory at the starting point of the internal carotid artery near the carotid sinus, which resulted in low shear stress. Oscillatory shear index (OSI) signifies oscillatory behavior wall shear stress. By using the anatomically realistic 3D geometry and representative physiological conditions, the results obtained for shear stress are more acceptable. Comparing the results of this study with available literature shows that the

regions with low wall shear stress and with OSI value more than 0.3 face potential risk to the plaque development. It is observed that hemodynamics of carotid artery is very much affected by the geometry and flow conditions and relatively low wall shear stress regions were observed post stenosis, which is a known reason for plaque development and progression.

Keywords: Carotid artery; Hemodynamics; Fluid Structure Interaction; Wall shear stress; Arterial deformation; Newtonian model; Hypertension; Normal Blood pressure; oscillatory shear index.

## 1. Introduction:

Atherosclerosis is the most common Cardiovascular Disease (CVD) causing increased morbidity in many industrialized countries. Although atherosclerosis is a general disease involving several factors, it preferentially affects the wall of the vessel bifurcations (Kwak et al., 2014). The reason behind this focal nature is due to the local hemodynamic factors such as Wall shear stress and flow recirculation in those regions(Fox, James, Morgan, & Seed, 1982) . Atherosclerosis in large arteries is one of the major causes of stroke and is a cause for high risk of death and leading to major disabilities. It is mainly caused by ischemia or hemorrhage. Weakened cerebral hemodynamics is closely associated with carotid stenosis and blocking. One of the symptoms is Transient Ischemic Attack (TIA). It was observed by Eliasziw et al (Eliasziw, Kennedy, Hill, Buchan, & Barnett, 2004) that patients who had a hemispheric TIA related to internal carotid artery disease had a high risk of stroke in the first few days after the TIA. Early risk of stroke was not affected by the degree of internal carotid artery stenosis. Stroke can also occur due to plaque rupture from a stenosed carotid artery, which is a perfect location for the development of atherosclerosis because of the arterial bifurcations leading to disturbed and complex flow (Markus, 2001). The significant role played by hemodynamic parameters such as blood pressure, Wall Shear Stress (WSS) in the formation and progression

of CVD (Eliasziw et al., 2004) makes it very essential to understand the hemodynamics in the carotid artery.

Blood is a non-Newtonian fluid, containing various components such as platelets, white blood cells, red blood cell, etc.(Bakker, 1991), however, researchers have considered blood as a Newtonian fluid because in large vessels (lumen diameter varying from 1 to 3 mm) the shear rates are higher than 100 $s^{-1}$(Javaid & Alfishawy, 2016; Jeziorska & Woolley, 1999; Norbert, Laurent, & Philippe, 2005; Torii, Oshima, Kobayashi, Takagi, & Tezduyar, 2006).

The arterial deformation is governed by linear momentum equations of the arterial wall which is influenced by the structural model used as well as the nature of the geometry (Torii, Oshima, Kobayashi, Takagi, & Tezduyar, 2009). The structural modeling of the artery is elaborately discussed in cardiovascular biomechanics (Fung & Skalak, 1981; Humphrey & Epstein, 2002). The simple way to model an artery is to assume the arterial material to be linearly elastic material. The advantage of this assumption is that it is computationally inexpensive and the results obtained by this approach agrees well with the experimental data within physiological pressure range (Torii, Oshima, Kobayashi, Takagi, & Tezduyar, 2007). This method is used in many application like small – on – large concept suggested by Baek et al (Baek, Gleason, Rajagopal, & Humphrey, 2007), where the artery is considered to be linearly elastic in physiological pressure range and useful in patient specific FSI simulations. Hyper elastic materials are also used widely in arterial mechanics and cardiovascular FSI computations (Bazilevs, Calo, Zhang, & Hughes, 2006; Di Martino & Vorp, 2003). The method enables the modeling of stiffening behavior and incompressibility of the wall under high strain conditions. More sophisticated arterial wall models are also adopted, considering the viscoelastic, inhomogeneous characteristics owing to compositions of the arterial wall (Humphrey & Epstein, 2002). Such models are desirable because the diseased artery compositions are more diverse and complicated (Gasser & Holzapfel, 2007). However, application of these material

models to patient specific studies are scarce because the arterial information such as composition, orientation of the fiber, lipid accumulation sites and calcification and its properties are difficult to obtain. Many researchers have used different elasticity models in their study, and have observed that when the arterial tissue is described by a nonlinear model, it behaves as a more rigid material than when it is modelled by the linear elastic model (Mengaldo et al., 2012) and the changes are not dramatic. Therefore, in patient specific FSI simulations, arterial wall is modelled as linearly elastic material. Rigid wall assumption overestimates the wall shear stress (WSS), sometimes by 50%, and it causes some qualitative and quantitative differences when compared with more accurate flexible wall approach. Therefore, use of elastic artery models are more appropriate (Bazilevs, Takizawa, & Tezduyar, 2013).

Another major cause of stroke is hypertension. Many studies were performed on the effect of hypertension on aneurysms and stenosed arteries. Researchers observed that hypertension increases the WSS and deformation in aneurysm regions, which is initiated by extreme stress - strain conditions (Yang et al., 2014), whereas Milad et al (Samaee, Tafazzoli-Shadpour, & Alavi, 2017) experimentally elucidated that the increase in stenosis severity in the carotid artery. This leads to increased negative WSS and oscillatory shear in the post stenosis region and increased angular phase difference between WSS and circumferential stress waves at the throat of the stenosis. All the parameters help predict the potential plaque growth locations and these results helped in studying the plaque growth and arterial remodeling (Janela, Moura, & Sequeira, 2010). To understand the effect of arterial compliance a two-way fluid structure interaction study was performed on a hypertensive case to understand the progression of atherosclerotic plaque in an arterial bifurcation (Agarwal, Katiyar, & Pradhan, 2008; Janela et al., 2010; Yao, Mamun Molla, & Ghosh Moulic, 2013). The effect of hypertension on the atherosclerotic arteries was studied as it poses a major risk in the rupture of the plaque (Rabby, Razzak, & Molla, 2013). A significant correlation between carotid strain parameters and peak

and mean WSS in hypertension was also observed (Eliasziw et al., 2004). Also, the intima media thickness in the common carotid artery and the carotid bulb is related to the blood pressure (Toloui, Firoozabadi, & Saidi, 2012). Corrada et al showed that the deformation of the wall was significantly influenced by hypertension and it is a risk factor based on FSI results. Blood pressure was classified into four stages, normal (120/80 mm Hg), prehypertension (120-139/80-89), stage 1 hypertension (140-159/90-99 mm Hg), stage 2 hypertension ($\geq 160/ \geq 100$ mm Hg) (Corrada et al., 2017).

Literature on the stenosed artery with the effect of blood pressure stages using the appropriate blood rheology are scarce. Vasava et al (Vasava, Jalali, Dabagh, & Kolari, 2012) studied a three-dimensional model of aortic arch using finite element method by considering the artery as rigid. Results comparing the effects of hypertension and hypotension was illustrated and showed that the low and oscillating shear stress at the walls of the aortic arch due to hypertension and hypotension play a significant role in the development of atherosclerosis.

In this study, a three-dimensional patient specific FSI study is performed on a human carotid artery with a partial occlusion in the External Carotid Artery (ECA) origin with normal Internal Carotid Artery (ICA) and Common Carotid Artery (CCA). The novelty of this work is to observe the effect of different stages of hypertension on the same anatomical geometry. The computational setup is simulated for three blood pressure cases as suggested (Corrada et al., 2017) viz., normal, prehypertension (HBP 1), hypertension stage 1 (HBP 2), hypertension stage 2 (HBP 3). The study is also conducted to observe the effect of vortex generation on WSS at different locations.

## 2. Methodology

### 2.1.Image acquisition and reconstruction.

A 3D model of patient specific carotid artery was constructed by selecting CT angio data followed by converting 2D CT scan images into 3D model using MIMICS 19 (Materialise, Leuven, Belgium) medical image processing software. To avoid the stair-step artifact that generally appears on the curved surface of the model, the scan interval was kept less than 2 mm. The developed model had more than 300 slices, each in coronal, sagittal, and axial planes. Using appropriate threshold ranging from -150 to 450 HU, the carotid artery was identified, and the segmentation process was carried out. Using automatic region growing, the carotid bifurcation was segmented as shown in Figure 1.

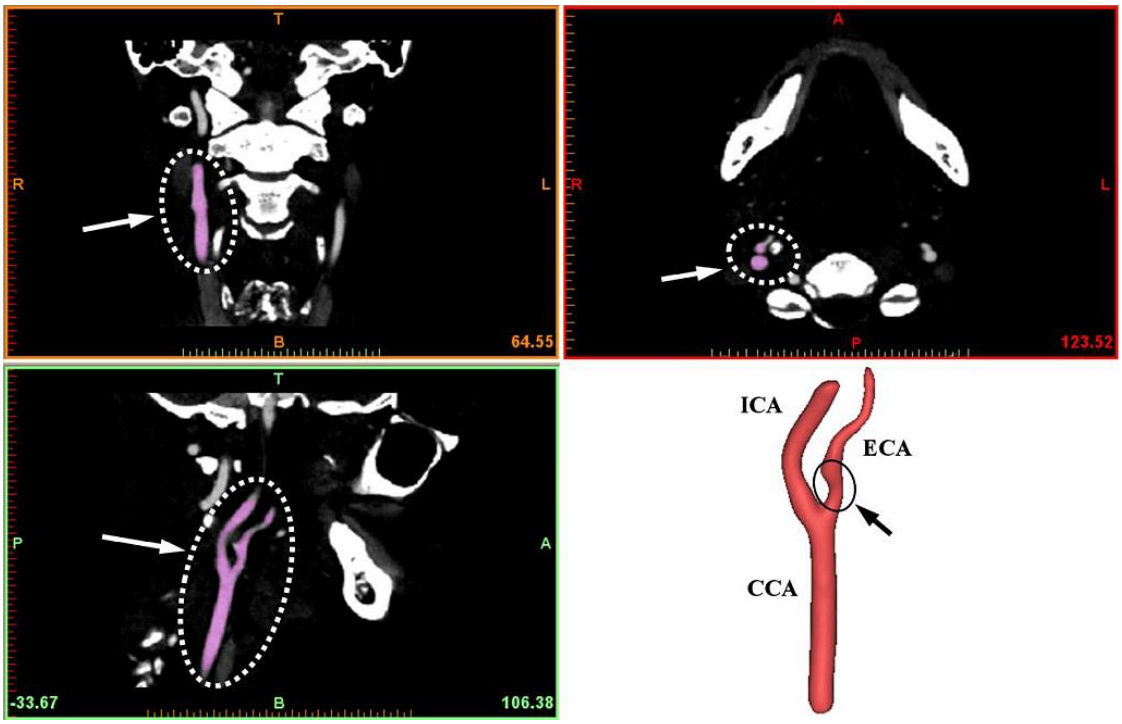


Figure 1: CT images from different planes and generated 3D model of the carotid bifurcation.

As the FSI model consists of fluid and structural model representing blood and elastic artery, both were generated separately. The usual range of carotid intima media is in the range of 0.6

to 0.8 mm (Hodis et al., 1998; Stein, 2004). In this study, the arterial wall thickness was assumed 0.7 mm.

### 2.2.Modelling and computational setup.

The general FSI problem involves the fluid and solid domains, interface conditions, and the relevant conditions for other boundaries. The fluid flow is considered laminar governed by the Navier – Stokes equations of incompressible flows in Arbitrary Lagrange Eulerian framework:

$$\rho_f \left(\frac{\partial v_f}{\partial t} + v.\nabla v\right) - \nabla.\sigma_f = 0, \nabla.v = 0 \text{ in fluid domain} \qquad (1)$$

Where ρ is constant density and *v* is the velocity of the field. The flow is described by pressure and velocity fields $p_f$ and $v_f$ respectively. The external forces like gravity or motion of the human body is considered not significant and hence neglected.

The constitutive relations for stress tensors read as

$$\sigma_f = -p_f I + 2\mu\varepsilon(v_f) \qquad (2)$$

Where $\mu$ is dynamic viscosity of the fluid, $p_f$ is the Lagrange multiplier corresponding to incompressibility constraint in (1), $\varepsilon(v_f)$ is the strain – rate tensor:

$$\varepsilon(v_f) = \frac{1}{2}\left(\nabla v_f + (\nabla v_f)^T\right) \qquad (3)$$

The governing equation for the structure is

$$\rho_s \left(\frac{\partial v_s}{\partial t} + (\nabla v_s)v_s - g\right) - \nabla.\sigma_s = 0 \quad \text{in } \Omega_t^s \qquad (4)$$

Where s denotes structure, $\rho_s$ is the material density, g represents the external body forces acting on the structure and $\sigma_s$ is the Cauchy stress tensor.

The structure configuration is described by the displacement $u_s$, with velocity field $v_s = \frac{\partial u_s}{\partial t}$. In a common lagrangian description with respect to some fixed reference state we have

$$\rho_s \left( \frac{\partial^2 u_s}{\partial t^2} - g \right) - \nabla . \Sigma_s = 0 \text{ in } \Omega_s, \qquad (5)$$

Where the tensor $\Sigma_s = J\sigma_s F^{-T}$ is called the first Piola – Kirchoff tensor (Kamali, Kheirandish, & Paktinat, 2018) is the momentum equation.

The boundary conditions on the fluid – solid interface is assumed to be

$$\sigma_f n = \sigma_s n, v_f = v_s \text{ on } \Gamma_t^0 \qquad (6)$$

Where n is a normal unit vector to the interface $\Gamma_t^0$. This implies no slip condition for flow and that the interface forces are balanced.

3D unsteady Naiver stokes equations were solved using Ansys CFX 19.0 and structural analysis was performed using Ansys Structural 19.0 module (Ansys Inc., Canonsburg, PA). To ensure stability of two-way transient FSI analysis, steady state FSI analysis is first performed with a convergence residual target of $10^{-5}$ using first order high-resolution scheme to stabilize the flow. When steady state coupling analysis is completed, two-way transient FSI analysis is performed using steady state results as initial conditions for both domains (Q. Zhang & Cen, 2016). A second order high-resolution scheme was utilized for FSI analysis to achieve higher order of accuracy using lower courant number.

The optimum range of 1 to 10 was set for external coupling iterations and mesh displacement control with convergence criteria of $10^{-4}$ (Vassen, DeVincenzo, Hirsch, & Leonard, 2011). The mass flux source coefficient was defined at the interface to achieve convergence and stability (*ANSYS, Inc. (2015) ANSYS CFX-Solver Theory Guide, Release 16.2.*, n.d.; Degroote, Haelterman, Annerel, & Vierendeels, 2009). Sufficiently large pressures is transferred at the interface from fluid to structure. Here, mass flux pressure coefficient technique was used with

a fixed number of stagger loops and varying values of source coefficients to achieve convergence.

Second order Rhie Chow scheme was used to obtain the velocity and pressure coupling (How, 1996; Rhie & Chow, 1983; Versteeg & Malalasekera, 2007; S. Zhang, Zhao, & Bayyuk, 2014). The simulation was run for three cardiac cycle of 0.8 seconds each with a time step of 0.008 seconds. As the Reynolds number is 443, 450, 386.5, 438.2 and 388 for NBP, LBP, HBP 1, HBP 2 and HBP 3 respectively, laminar model was selected. A high-resolution advection scheme was used with second order backward Euler discretization algorithm.

## 3. Boundary Conditions:

A three-dimensional carotid artery was studied to elucidate the hemodynamics under different blood pressure conditions. Blood was considered as Newtonian with a dynamic viscosity of 0.004 Pa-s and artery as a linearly elastic model with Young's modulus of 0.9 MPa and Poisson's ratio of 0.45 since arterial wall undergoes small deformation of approximately 10 – 15% of mean diameter (Bella et al., 2012; Cho, Kim, Sung, Rou, & Ryou, 2011; Salzar, Thubrikar, & Eppink, 1995). The assumption of linear elastic model for the arterial wall has been shown to be computationally inexpensive and produce results that are in good agreement with the experimental data within physiological pressure range (Torii et al., 2007). A section from a long artery was considered in this study, therefore in structural model nodes at the ends were fixed so that the model remain stable during the pulsatile flow. The remaining nodes are free to move due to the fluid interaction with the structure (Misiulis, Džiugys, Navakas, & Striūgas, 2017; Tang, Yang, & Ku, 1999). A pulsatile velocity obtained from Doppler ultrasound was applied at the inlet. Resistance boundary condition was applied at the outlet

(Torii, Oshima, Kobayashi, Takagi, & Tezduyar, 2008). Figure 2 shows the 3D geometry and the boundary conditions applied.

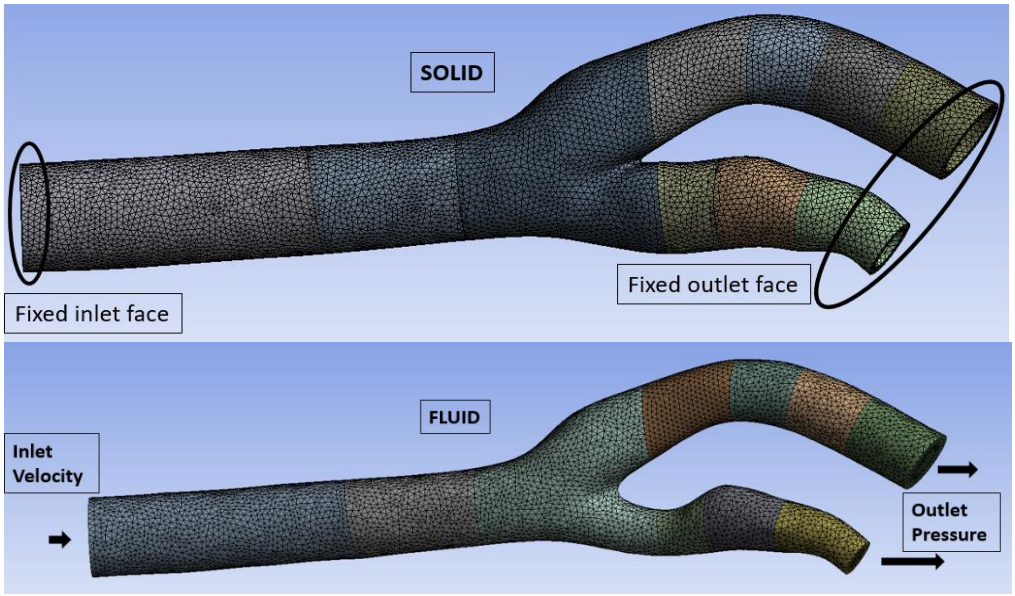


Figure 2: Boundary condition details 3D FSI model

Blood flow velocity was acquired by measuring the velocity components at the common carotid artery after the data was synchronized with the cardiac cycle. A slice at the CCA was chosen to quantify the flow. After segmentation of the arterial lumen, the velocity waveform was integrated over the lumen inlet. Figure 3 shows the velocity profile at the common carotid artery chosen.

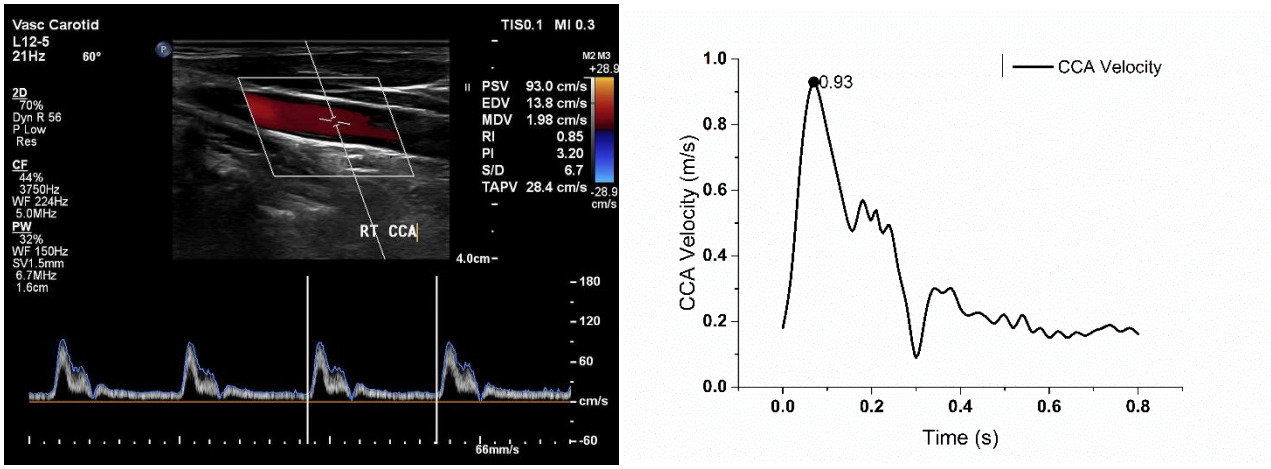


Figure 3: Ultrasound Doppler image to acquire the velocity at the inlet and corresponding velocity profile

Researchers have investigated different outlet boundary conditions (Gijsen, Allanic, Van De Vosse, & Janssen, 1999; Tu & Deville, 1996) like impedance, resistance, and constant pressure outlet. However, Torii et al (Torii et al., 2008) suggested that resistance pressure boundary condition as shown in equation at the outlet for many FSI studies. In this study resistance pressure boundary condition was used to consider the peripheral resistance encountered by the downstream arteries given by equation 7 (Torii et al., 2008).

$$P = P_0 + QR \qquad (7)$$

Where Q is the total outflow, $P_0$ is the reference pressure and R is the resistance due to distal vascular tree. A pulsatile pressure waveform as shown in Figure 4 was applied at the outlets. For both velocity inlet and pressure outlet, the obtained values are used to generate a polynomial equation and this data obtained was used in the Fourier series equation to generate the required pulse wave. The required Fourier coefficients for velocity and pressure were extracted from initial approximate waveforms and six harmonics, which is enough to obtain the desired pulsatile waves. A no - slip boundary condition is defined at the walls of the fluid model.

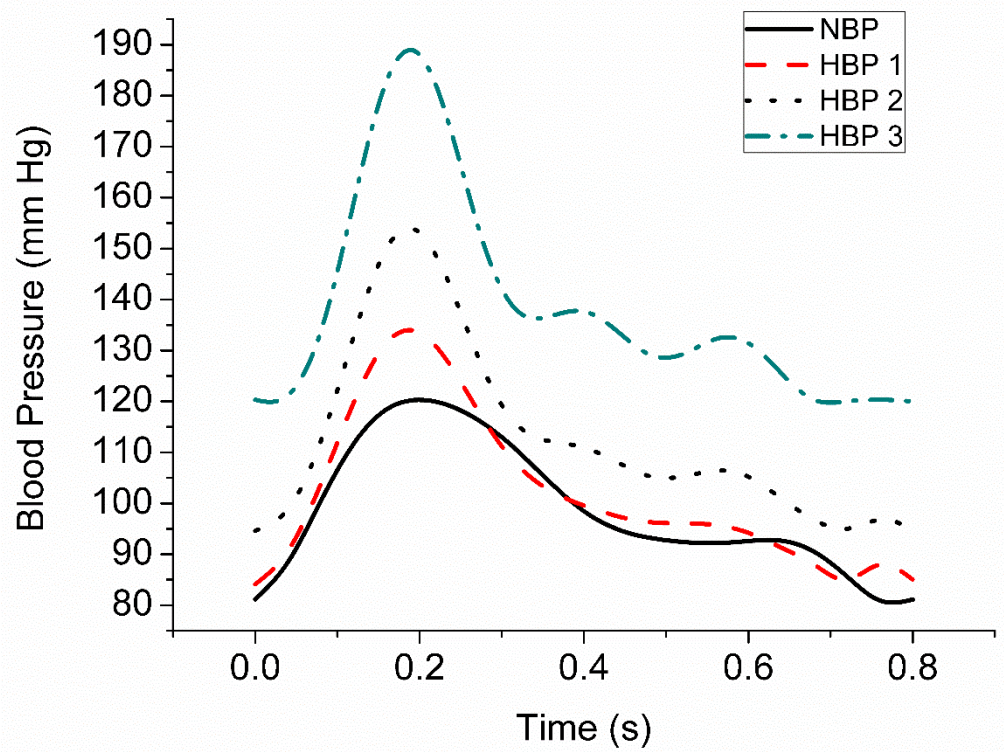


Figure 4: Representation of pulsatile pressure at the outlet

## 4. Results:

In this study, pulsatile blood flow is considered and hemodynamic parameters around and near the stenosis such as wall deformation, wall shear stress and flow velocity is explained at different time intervals of the cardiac cycle, different blood pressure conditions.

Grid independence study was carried out to choose optimum mesh size for the simulation. Figure 5 shows the variation of average deformation and average velocity for different grid

size. An optimum mesh size of 205938 and 215208 elements for structure and fluid respectively was chosen in study.

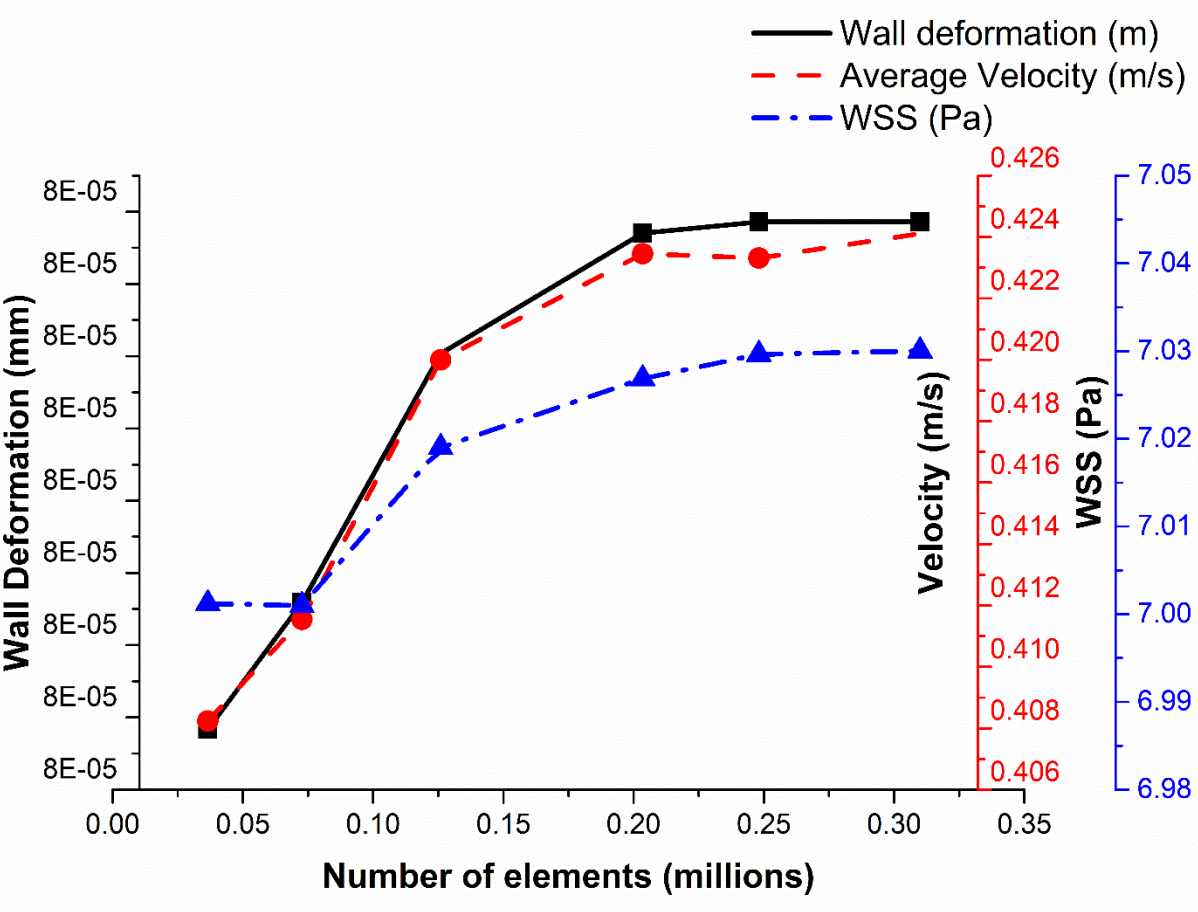


Figure 5: Grid independence study

To choose an optimum time step for FSI simulation, a transient time - step sensitivity test is performed. Transient analysis is carried out for different time steps starting with 25, 50, 100 and 200 steps with step size of 0.032s, 0.016s, 0.008s and 0.0064s respectively and average velocity and average WSS is plotted at different time - steps as shown in Figure 6. Based on the time – step sensitivity test, FSI simulations with 100 time steps with a step size of 0.008 s is performed.

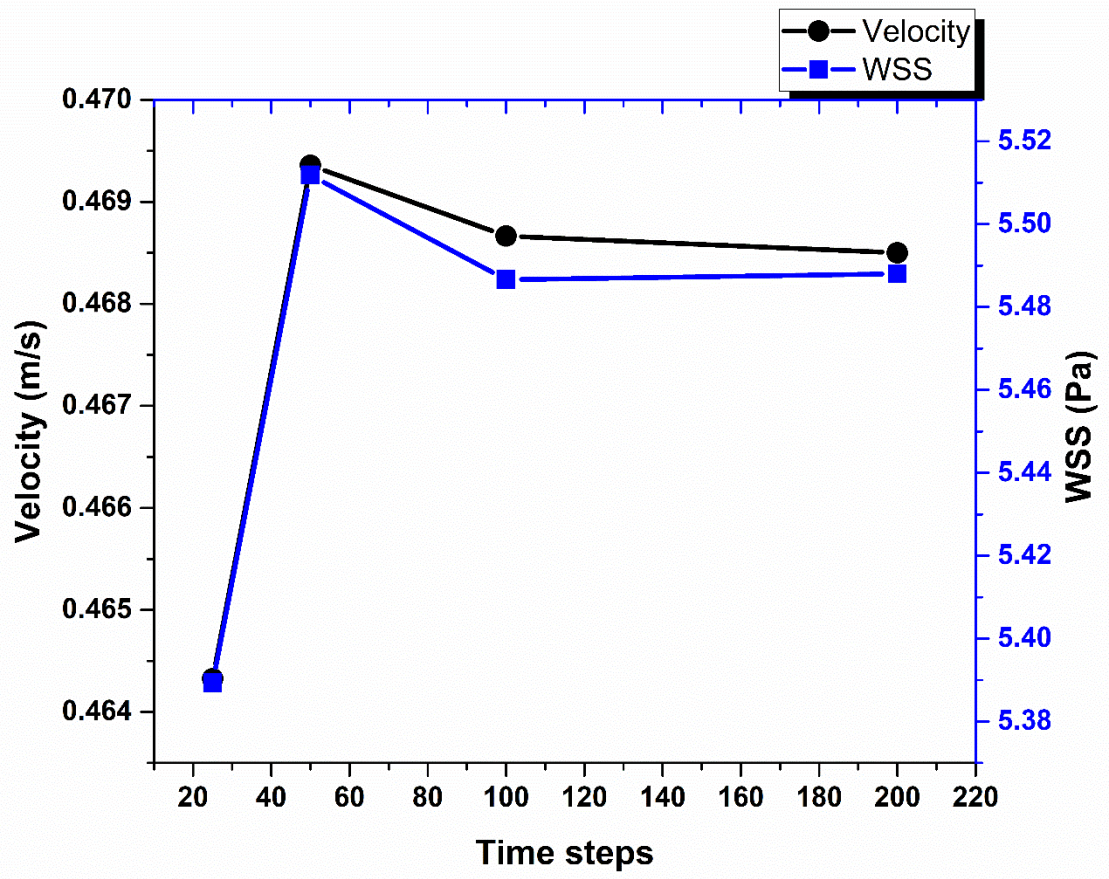


Figure 6: Time step sensitivity test

### 4.1.Wall deformation

Figure 6 shows percentage increase in deformation at different time intervals and different blood pressure condition. As expected, the deformation is increasing with the increase in blood pressure during peak systole. This increase in deformation enlarges the artery, which reduced the wall shear stress and increasing the recirculation zone. The deceleration of flow after peak, a large recirculation zone is developed at the non-divider wall due to the stored elastic energy in the elastic arterial wall.

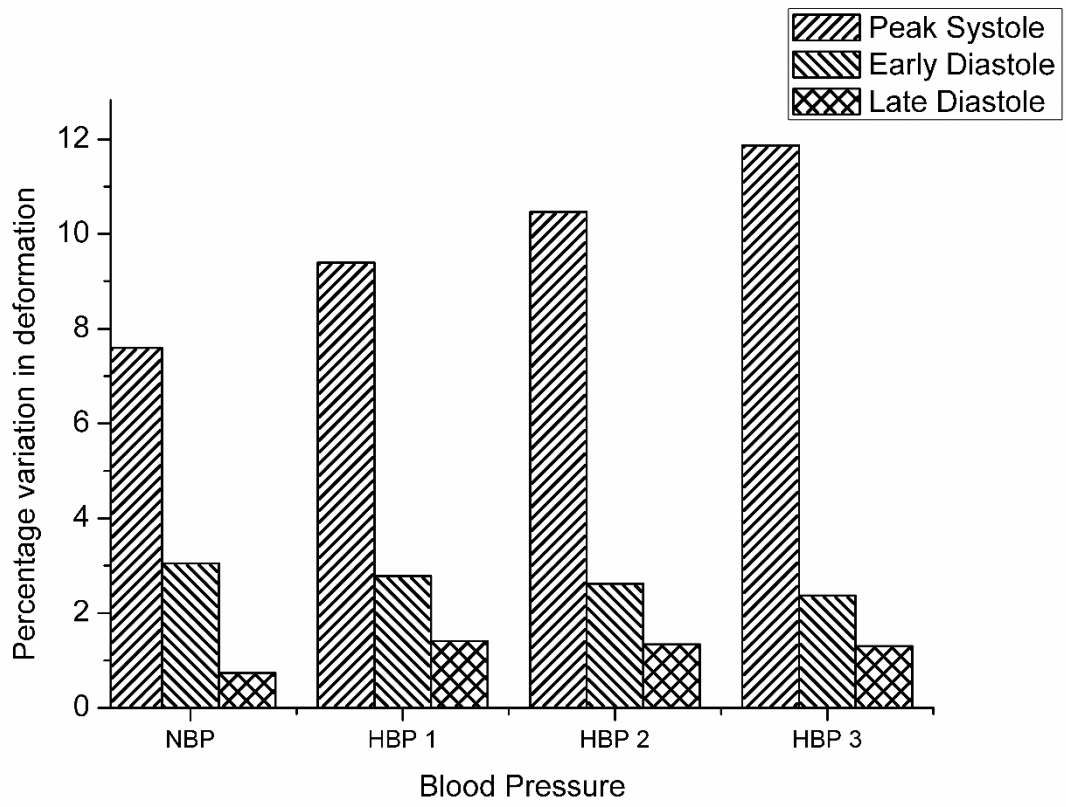


Figure 7: Percentage variation in deformation compared to initial state.

Figure 7 shows the variation of deformation at Plane 1 to 4 for the different BP cases. Maximum deformation occurs at plane 1 near the carotid sinus. There was no noticeable change in the deformation magnitude at plane 3 and 4.

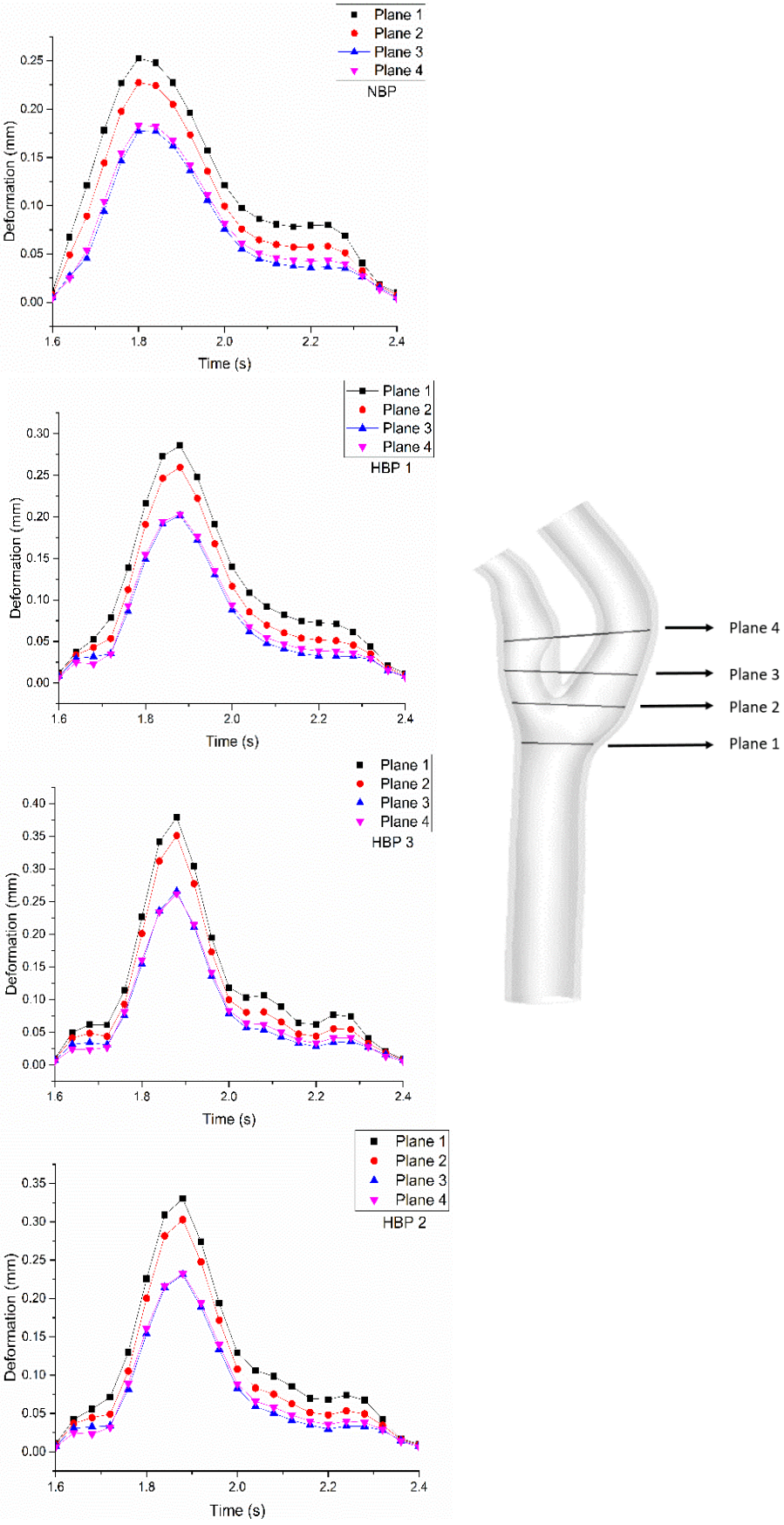


Figure 8: Variation of deformation along different planes

### 4.2.Wall shear stress

Figure 8 shows the temporal variation of WSS for different blood pressures. It can be observed that for NBP condition the WSS variation is proportional to the pressure variation. However, for HBP 2 and HBP 3 condition, the WSS behaves in an oscillatory fashion with a reduction in the WSS magnitude at peak systole. Figure 9 shows Wall Shear Stress contours for NBP, HBP 1, HBP 2 and HBP 3 at peak systole, early diastole and late diastole. Maximum WSS magnitude for NBP, HBP 1, HBP 2 and HBP 3 are 10.147 Pa, 10.176 Pa, 9.858 Pa and 9.631 Pa respectively. Table 2 shows the WSS magnitude at different BP cases. The WSS magnitude increases with increasing blood pressure and at late diastole, the WSS tends to concentrate mainly near the stenosis region at the bifurcation and at the inner wall of the ICA as shown in Figure 9. At peak systole, the WSS is concentrated mainly at the inner wall of ICA at the curved region, whereas the low WSS region is predominant immediately after stenosis for all cases. The intensity of low shear region increases at early diastole and it spreads all over the inner wall of ECA at late diastole. In addition, at this instant WSS increases pre stenosis at the neck of the stenosis. Low WSS is also observed at the carotid sinus and post stenosis region due to flow recirculation caused by increased diameter.

Table 1: Maximum WSS magnitudes

| BP | Maximum WSS (Pa) | | |
|---|---|---|---|
| | Peak Systole | Early Diastole | Late Diastole |
| NBP | 10.155 | 3.93 | 2.57 |
| HBP 1 | 10.176 | 4.171 | 2.58 |
| HBP 2 | 9.856 | 4.107 | 2.608 |
| HBP 3 | 9.631 | 4.03 | 2.74 |

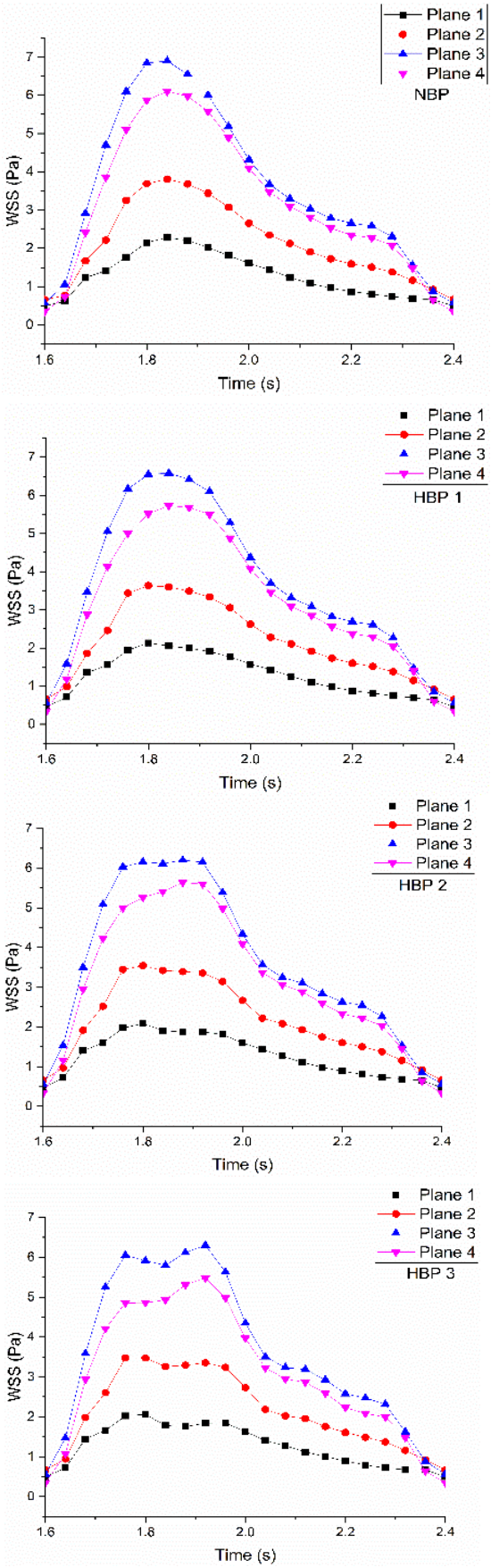


Figure 9: Temporal variation of WSS at different planes and for different BP conditions.

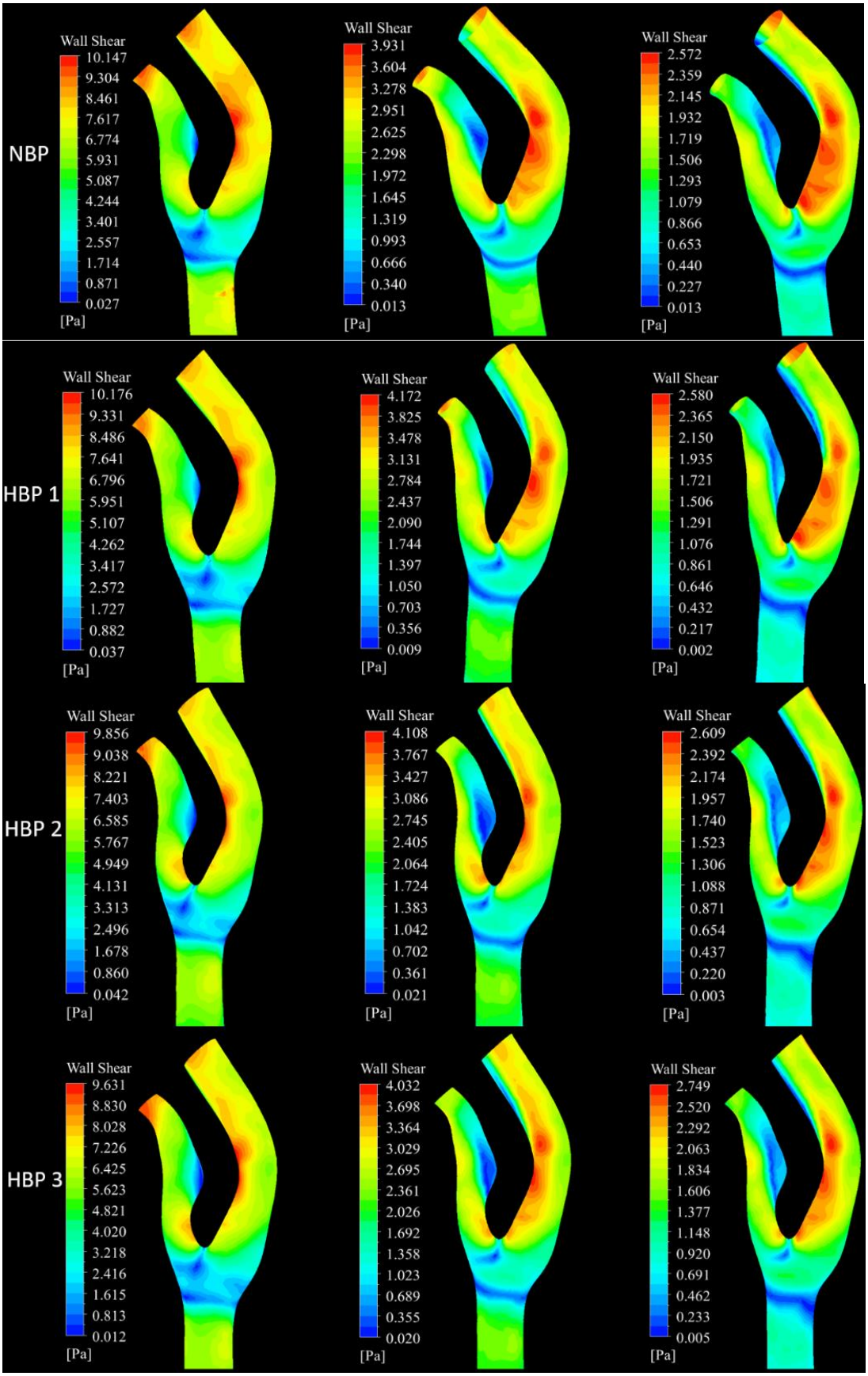


Figure 10: Wall shear stress contours for different blood pressure conditions at different stages of cardiac cycle.

### 4.3.Velocity

Figure 10 shows velocity streamlines for all the BP cases at different time intervals. The flow is uniform at peak systole, but at early diastole and late diastole, the flow turns chaotic post stenosis. The velocity magnitude is reduced with an increase in blood pressure at peak systole and it tends to increase at late diastole at ICA. The flow recirculation region is increased with higher blood pressure at late diastole.

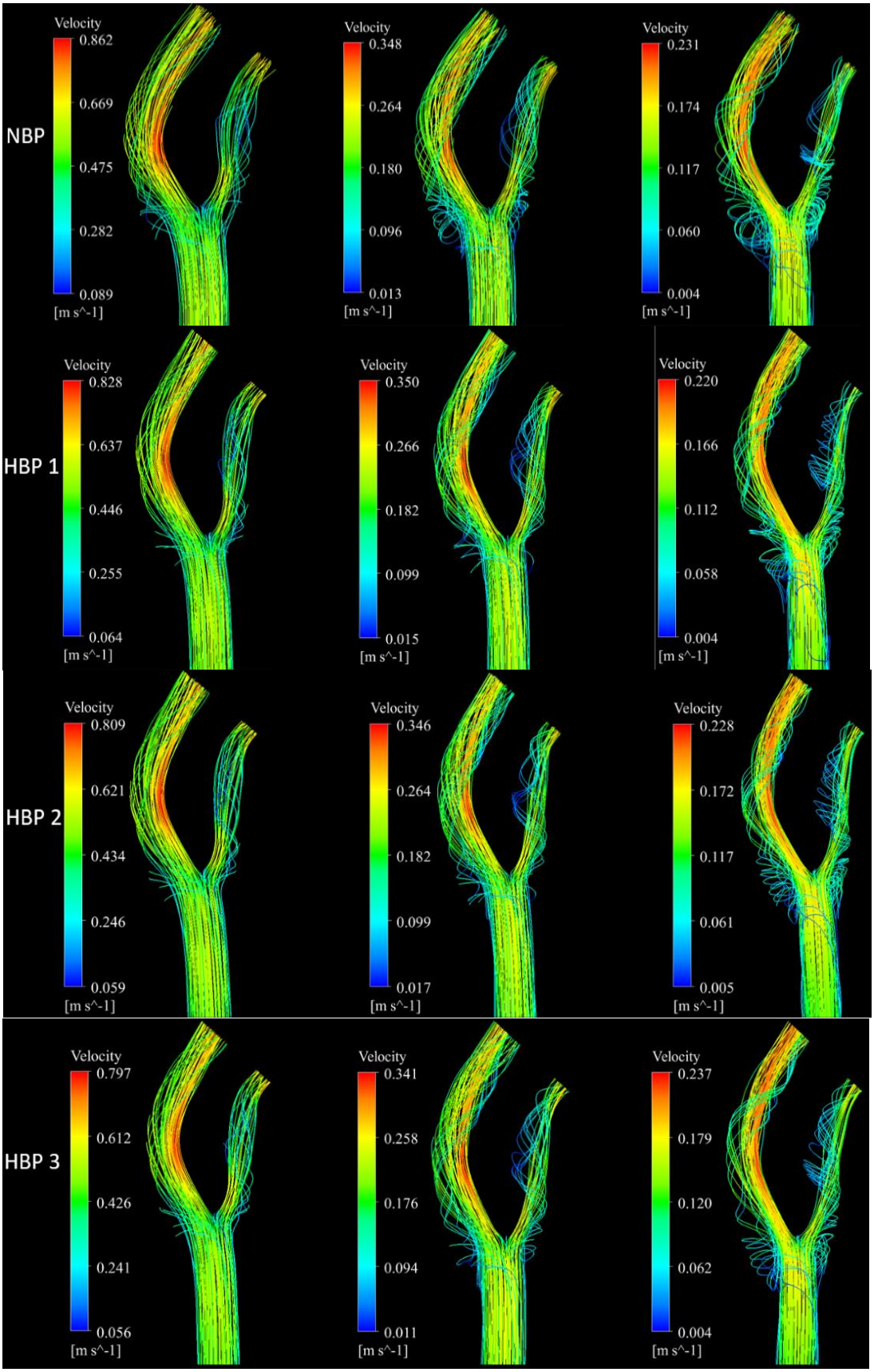


Figure 11: Wall shear stress contours for different blood pressure conditions at different stages of cardiac cycle.

### 4.4.Oscillatory Shear Index

The oscillatory shear index is a non-dimensional parameter used to evaluate the oscillatory behavior of arterial flows. It displays the differences between average WSS and average WSS vector. Using these values, the OSI elucidates the WSS vector deflection from blood flow principal directions during cardiac cycle. Therefore, OSI is calculated

$$OSI = 0.5 \times \left(1 - \frac{\left|\int_0^T \overrightarrow{WSS} dt\right|}{\int_0^T |\overrightarrow{WSS}| dt}\right) \qquad (8)$$

Where $\left|\overrightarrow{WSS}\right|$ is the instantaneous WSS (N/m$^2$) magnitude and T (sec) is the cardiac cycle time. The OSI can range from 0 for no variations and to 0.5 for $180^0$ deflection in WSS (Soulis, Lampri, Fytanidis, & Giannoglou, 2011). The variation of OSI for different blood pressures is shown in Figure 10. HBP 3 shows the highest value of OSI, which co-relates with high oscillatory behavior of WSS as shown in Figure 9, however, the difference in the magnitude of the OSI between different cases, is marginal.

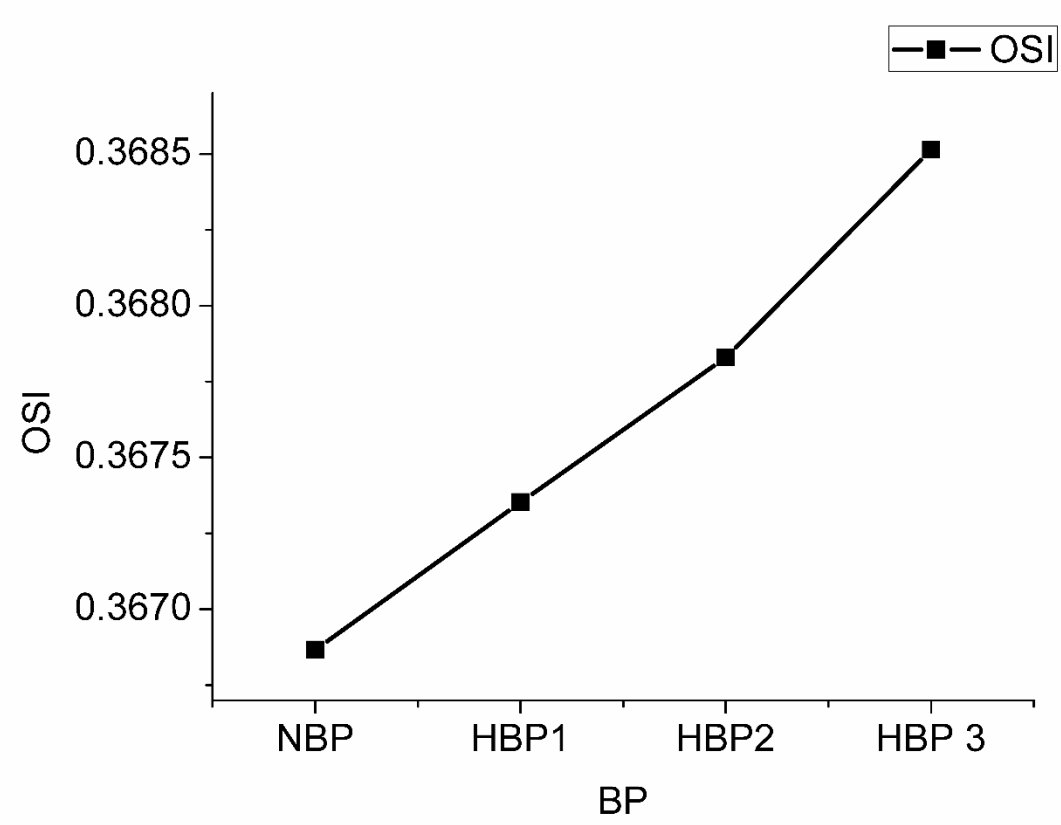


Figure 12: Oscillatory shear index for different blood pressure

## 5. Discussion:

In this study, flow parameters at varying blood pressures in a stenosed carotid artery are evaluated. At the downstream of the stenosis, flow separation was observed leading to vortices, however, vortex shedding was observed at elevated flow rates due to the increased momentum of flow, which separates large eddies into smaller ones and in turn releasing kinetic energy. At peak systole, higher velocity was observed pre-stenosis in ECA and flow separation occurring immediately post stenosis region. The velocity magnitude was inversely proportional to the variation in blood pressure. This was due to higher peripheral resistance due to blood pressure, which also leads to an increase in arterial deformation. Flow velocity was increased at ICA at late diastole as the increased flow recirculation resists flow in ECA.

Variations in WSS was evaluated at different blood pressures. It can be observed that the WSS magnitude was low at HBP 3 and high at LBP at peak systole. At the bifurcation, the flow in

the downstream leading to large contact areas of the arterial wall leading to increased WSS as seen in Figure 9. Due to the increased flow rate the contact intensity increases leading to increased shear rate at the wall surface, making this region favorable for plaque rupture. As the stenosis is in the external carotid artery, its effect on the healthy branch is also greater due to the law of conservation of mass. Presence of stenosis in ECA makes the ICA a favorable location for stenosis generation because of the generation of flow recirculation at the carotid sinus. These observations lead to a more concentrated qualitative measurement of WSS based descriptors on the arterial wall. Wall shear stress is a flow driven parameter. Therefore, the variation in blood pressure also governs the WSS variation. Since the flow is in the axial direction, the value of WSS is more in axial direction compared to the other directions. However, at high flow rates oscillatory behavior of the WSS may be due to chaotic flow developed due to the interaction of blood and the stenosed region of the arterial wall, such interactions create unstable flow domains in the flow direction, leading to significant flow in a direction perpendicular to the direction of flow. Therefore, based on the WSS markers, the locations prone to secondary plaque accumulation can be evaluated. The projected WSS as shown in Figure 8 shows high values at the bifurcation and at the throat of the stenosis for all BP cases. Low values are observed at the downstream region of the stenosis, particularly at the inner wall of the ECA. The average WSS plots shown in Figure 8 brings out the differences in temporal WSS variations for different BP cases. The normal BP has a proportionate variation compared to the pressure, as the BP increases the oscillatory behavior is more evident.

To support this oscillatory behavior of WSS oscillatory shear index is calculated. Although the difference in the magnitude is marginal between different blood pressures, a higher value of OSI for HBP 3 supports the oscillatory behavior of WSS as shown in Figure 11. OSI show a significantly high sensitivity in HBP 2 and HBP 3 cases than other cases. This can be attributed to the areas with low WSS.

## 6. Conclusion:

In this study, the pulsatile flow of blood considered as Newtonian fluid in the carotid artery, with different physiological pressure conditions and with the effect of fluid structure interaction was studied. In past studies, computational and clinical studies were conducted to study the wall shear stress distribution and its oscillatory behavior in arteries (Soulis et al., 2011). The change in direction of OSI cause cell proliferation in the vasculature. By studying the OSI in arteries gives a better perception of flow changes in the arteries. Since the artery is stenosed, the chances of increase in plaque deposition are more irrespective of blood pressure.

The decrease in the WSS is observed post stenotic region and the region of low WSS closely related with vascular atherosclerosis is determined. It was observed that under high distal vascular resistance the artery is subjected to low WSS, which related to plaque progression. With low distal vascular resistance, the artery is subjected to considerably higher WSS.

The results of this study demonstrate the potential of Computational Fluid Dynamics (CFD) techniques in the further understanding of the causes of CVD and pave the way in the creation of innovative computational solutions in aiding the early diagnosis of atherosclerosis.

## References

Agarwal, R., Katiyar, V. K., & Pradhan, P. (2008). A mathematical modeling of pulsatile flow in carotid artery bifurcation. *International Journal of Engineering Science*, *46*(11), 1147–1156. https://doi.org/https://doi.org/10.1016/j.ijengsci.2008.06.002

*ANSYS, Inc. (2015) ANSYS CFX-Solver Theory Guide, Release 16.2.* (n.d.). Retrieved from http://read.pudn.com/downloads500/ebook/2077964/cfx_mod.pdf

Baek, S., Gleason, R. L., Rajagopal, K. R., & Humphrey, J. D. (2007). Theory of small on

large: potential utility in computations of fluid--solid interactions in arteries. *Computer Methods in Applied Mechanics and Engineering*, *196*(31–32), 3070–3078.

Bakker, P. G. (1991). *Bifurcations in Flow Patterns Nonlinear Topics in the Mathematical Sciences*. Springer, Dordrecht. https://doi.org/10.1007/978-94-011-3512-2

Bazilevs, Y., Calo, V. M., Zhang, Y., & Hughes, T. J. R. (2006). Isogeometric fluid--structure interaction analysis with applications to arterial blood flow. *Computational Mechanics*, *38*(4–5), 310–322.

Bazilevs, Y., Takizawa, K., & Tezduyar, T. E. (2013). *Computational fluid-structure interaction: methods and applications*. John Wiley & Sons.

Bella, J. N., Roman, M. J., Pini, R., Schwartz, J. E., Pickering, T. G., & Devereux, R. B. (2012). Assessment of Arterial Compliance by Carotid Midwall Strain-Stress Relation in Hypertension. *Hypertension*, *33*(3), 793–799. https://doi.org/10.1161/01.hyp.33.3.793

Cho, S. W., Kim, S. W., Sung, M. H., Rou, K. C., & Ryou, H. S. (2011). Fluid-structure interaction analysis on the effects of vessel material properties on blood flow characteristics in stenosed arteries under axial rotation. *Korea Australia Rheology Journal*, *23*(1), 7–16. https://doi.org/10.1007/s13367-011-0002-x

Corrada, M. M., Hayden, K. M., Paganini-Hill, A., Bullain, S. S., DeMoss, J., Aguirre, C., … Kawas, C. H. (2017). Age of onset of hypertension and risk of dementia in the oldest-old: The 90+ Study. *Alzheimer's and Dementia*, *13*(2), 103–110. https://doi.org/10.1016/j.jalz.2016.09.007

Degroote, J., Haelterman, R., Annerel, S., & Vierendeels, J. (2009). Coupling techniques for partitioned fluid-structure interaction simulations with black-box solvers. In *10th MpCCI User Forum* (pp. 82–91).

Di Martino, E. S., & Vorp, D. A. (2003). Effect of variation in intraluminal thrombus constitutive properties on abdominal aortic aneurysm wall stress. *Annals of Biomedical Engineering*, *31*(7), 804–809.

Eliasziw, M., Kennedy, J., Hill, M. D., Buchan, A. M., & Barnett, H. J. M. (2004). Early risk of stroke after a transient ischemic attack in patients with internal carotid artery disease. *Canadian Medical Association Journal*, *170*(7), 1105 LP – 1109. https://doi.org/10.1503/cmaj.1030460

Fox, B., James, K., Morgan, B., & Seed, A. (1982). Distribution of fatty and fibrous plaques in young human coronary arteries. *Atherosclerosis*, *41*(2–3), 337–347. https://doi.org/10.1016/0021-9150(82)90198-8

Fung, Y., & Skalak, R. (1981). Biomechanics: mechanical properties of living tissues. American Society of Mechanical Engineers Digital Collection.

Gasser, T. C., & Holzapfel, G. A. (2007). Finite element modeling of balloon angioplasty by considering overstretch of remnant non-diseased tissues in lesions. *Computational Mechanics*, *40*(1), 47–60.

Gijsen, F. J. H., Allanic, E., Van De Vosse, F. N., & Janssen, J. D. (1999). The influence of the non-Newtonian properties of blood on the flow in large arteries: Unsteady flow in a 90°curved tube. *Journal of Biomechanics*, *32*(7), 705–713. https://doi.org/10.1016/S0021-9290(99)00014-7

Hodis, H. N., Mack, W. J., LaBree, L., Selzer, R. H., Liu, C., Liu, C., & Azen, S. P. (1998). The role of carotid arterial intima-media thickness in predicting clinical coronary events. *Annals of Internal Medicine*, *128*(4), 262–269.

How, T. V. (1996). *Advances in hemodynamics and hemorheology. Volume 1*. JAI Press.

Humphrey, J. D., & Epstein, M. (2002). Cardiovascular solid mechanics: cells, tissues, and organs. American Society of Mechanical Engineers Digital Collection.

Janela, J., Moura, A., & Sequeira, A. (2010). A 3D non-Newtonian fluid–structure interaction model for blood flow in arteries. *Journal of Computational and Applied Mathematics*, *234*(9), 2783–2791. https://doi.org/https://doi.org/10.1016/j.cam.2010.01.032

Javaid, A., & Alfishawy, M. (2016). Internal Carotid Artery Stenosis Presenting with Limb Shaking TIA. *Case Reports in Neurological Medicine*, *2016*(Figure 1), 1–4. https://doi.org/10.1155/2016/3656859

Jeziorska, M., & Woolley, D. E. (1999). Local neovascularization and cellular composition within vulnerable regions of atherosclerotic plaques of human carotid arteries. *The Journal of Pathology*, *188*(2), 189–196. https://doi.org/10.1002/(SICI)1096-9896(199906)188:2<189::AID-PATH336>3.0.CO;2-N

Kamali, R., Kheirandish, S., & Paktinat, K. (2018). Investigation of Different Activities on the Hemodynamic Parameters of Left External Carotid Artery Using Fluid–Structure Interaction. *Iranian Journal of Science and Technology, Transactions of Mechanical Engineering*, *4*(2012). https://doi.org/10.1007/s40997-018-0142-4

Kwak, B. R., Bäck, M., Bochaton-Piallat, M.-L., Caligiuri, G., Daemen, M. J. A. P., Davies, P. F., … Evans, P. C. (2014). Biomechanical factors in atherosclerosis: mechanisms and clinical implications†. *European Heart Journal*, *35*(43), 3013–3020. https://doi.org/10.1093/eurheartj/ehu353

Markus, H. (2001). Severely impaired cerebrovascular reactivity predicts stroke and TIA risk in patients with carotid artery stenosis and occlusion. *Brain*, *124*(3), 457–467. https://doi.org/10.1093/brain/124.3.457

Mengaldo, G., Tricerri, P., Crosetto, P., Deparis, S., Nobile, F., & Formaggia, L. (2012). A comparative study of different nonlinear hyperelastic isotropic arterial wall models in patient-specific vascular flow simulations in the aortic arch. MOX-Report.

Misiulis, E., Džiugys, A., Navakas, R., & Striūgas, N. (2017). A fluid-structure interaction model of the internal carotid and ophthalmic arteries for the noninvasive intracranial pressure measurement method. *Computers in Biology and Medicine*, *84*, 79–88. https://doi.org/https://doi.org/10.1016/j.compbiomed.2017.03.014

Norbert, N., Laurent, D., & Philippe, D. (2005). The Vulnerable Carotid Artery Plaque. *Stroke*, *36*(12), 2764–2772. https://doi.org/10.1161/01.STR.0000190895.51934.43

Rabby, M. G., Razzak, A., & Molla, M. M. (2013). Pulsatile Non-Newtonian Blood Flow through a Model of Arterial Stenosis. *Procedia Engineering*, *56*, 225–231. https://doi.org/https://doi.org/10.1016/j.proeng.2013.03.111

Rhie, C. M., & Chow, W. L. (1983). Numerical study of the turbulent flow past an airfoil with trailing edge separation. *AIAA Journal*, *21*(11), 1525–1532.

Salzar, R. S., Thubrikar, M. J., & Eppink, R. T. (1995). Pressure-induced mechanical stress in the carotid artery bifurcation: A possible correlation to atherosclerosis. *Journal of Biomechanics*, *28*(11), 1333–1340. https://doi.org/10.1016/0021-9290(95)00005-3

Samaee, M., Tafazzoli-Shadpour, M., & Alavi, H. (2017). Coupling of shear–circumferential stress pulses investigation through stress phase angle in FSI models of stenotic artery using experimental data. *Medical and Biological Engineering and Computing*, *55*(8), 1147–1162. https://doi.org/10.1007/s11517-016-1564-z

Soulis, J. V, Lampri, O. P., Fytanidis, D. K., & Giannoglou, G. D. (2011). Relative residence time and oscillatory shear index of non-Newtonian flow models in aorta. In *2011 10th*

*International Workshop on Biomedical Engineering* (pp. 1–4). https://doi.org/10.1109/IWBE.2011.6079011

Stein, J. H. (2004). Carotid intima-media thickness and vascular age: You are only as old as your arteries look. *Journal of the American Society of Echocardiography*, *17*(6), 686–689. https://doi.org/10.1016/j.echo.2004.02.021

Tang, D., Yang, C., & Ku, D. N. (1999). A 3-D thin-wall model with fluid–structure interactions for blood flow in carotid arteries with symmetric and asymmetric stenoses. *Computers & Structures*, *72*(1), 357–377. https://doi.org/https://doi.org/10.1016/S0045-7949(99)00019-X

Toloui, M., Firoozabadi, B., & Saidi, M. S. (2012). A numerical study of the effects of blood rheology and vessel deformability on the hemodynamics of carotid bifurcation. *Scientia Iranica*, *19*(1), 119–126. https://doi.org/https://doi.org/10.1016/j.scient.2011.12.008

Torii, R., Oshima, M., Kobayashi, T., Takagi, K., & Tezduyar, T. E. (2006). Fluid-structure interaction modeling of aneurysmal conditions with high and normal blood pressures. *Computational Mechanics*, *38*(4–5), 482–490. https://doi.org/10.1007/s00466-006-0065-6

Torii, R., Oshima, M., Kobayashi, T., Takagi, K., & Tezduyar, T. E. (2007). Influence of wall elasticity in patient-specific hemodynamic simulations. *Computers & Fluids*, *36*(1), 160–168.

Torii, R., Oshima, M., Kobayashi, T., Takagi, K., & Tezduyar, T. E. (2008). Fluid-structure interaction modeling of a patient-specific cerebral aneurysm: Influence of structural modeling. *Computational Mechanics*, *43*(1), 151–159. https://doi.org/10.1007/s00466-008-0325-8

Torii, R., Oshima, M., Kobayashi, T., Takagi, K., & Tezduyar, T. E. (2009). Fluid--structure interaction modeling of blood flow and cerebral aneurysm: significance of artery and aneurysm shapes. *Computer Methods in Applied Mechanics and Engineering*, *198*(45–46), 3613–3621.

Tu, C., & Deville, M. (1996). Pulsatile flow of non-Newtonian fluids through arterial stenoses. *Journal of Biomechanics*, *29*(7), 899–908. https://doi.org/https://doi.org/10.1016/0021-9290(95)00151-4

Vasava, P., Jalali, P., Dabagh, M., & Kolari, P. J. (2012). Finite element modelling of pulsatile blood flow in idealized model of human aortic arch: Study of hypotension and hypertension. *Computational and Mathematical Methods in Medicine*, *2012*. https://doi.org/10.1155/2012/861837

Vassen, J.-M., DeVincenzo, P., Hirsch, C., & Leonard, B. (2011). Strong coupling algorithm to solve fluid-structure-interaction problems with a staggered approach. In *7th European symposium on aerothermodynamics* (Vol. 692, p. 128).

Versteeg, H. K. (Henk K., & Malalasekera, W. (Weeratunge). (2007). *An introduction to computational fluid dynamics : the finite volume method*. Pearson Education Ltd. Retrieved from https://books.google.co.in/books/about/An_Introduction_to_Computational_Fluid_D.html?id=RvBZ-UMpGzIC

Yang, J., Cho, K., Kim, J., Kim, S., Kim, C., You, G., … Lee, J. (2014). Wall shear stress in hypertensive patients is associated with carotid vascular deformation assessed by speckle tracking strain imaging. *Clinical Hypertension*, *20*(1), 10. https://doi.org/10.1186/2056-5909-20-10

Yao, L.-S., Mamun Molla, M., & Ghosh Moulic, S. (2013). Fully-Developed Circular-Pipe

Flow of a Non-Newtonian Pseudoplastic Fluid. *Universal Journal of Mechanical Engineering*, *1*(2), 23–31. https://doi.org/10.13189/ujme.2013.010201

Zhang, Q., & Cen, S. (Eds.). (2016). 12 - Bidirectional multiphysics simulation of turbine machinery. In *Multiphysics Modeling* (pp. 340–348). Oxford: Academic Press. https://doi.org/https://doi.org/10.1016/B978-0-12-407709-6.00001-8

Zhang, S., Zhao, X., & Bayyuk, S. (2014). Generalized formulations for the Rhie--Chow interpolation. *Journal of Computational Physics*, *258*, 880–914.